PIEZO1 expression at the glio-vascular unit adjusts to neuroinflammation in seizure conditions

Valentin Garcia, Marine Blaquiere, Alicia Janvier, Noemie Cresto, Carla Lana, Athenais Genin, Hélène E. Hirbec, Etienne Audinat, Adèle Faucherre, Emmanuel Barbier, et al.

PIEZO1 expression at the glio-vascular unit adjusts to neuroinflammation in seizure conditions.

Valentin Garcia[1]*, Marine Blaquiere[1]*, Alicia Janvier[1], Noemie Cresto[1], Carla Lana[1], Athenais Genin[1], Helene Hirbec[1], Etienne Audinat[1], Adele Faucherre[1], Emmanuel L. Barbier[2], Sophie Hamelin[2], Philippe Kahane[2], Chris Jopling[1] and Nicola Marchi[1].

[1]Institute of Functional Genomics, University of Montpellier, CNRS, INSERM, Montpellier, France.
[2] Univ. Grenoble Alpes, Inserm, CHU Grenoble Alpes, Grenoble Institute Neuroscience, U1216, Grenoble, France.

*Equal contributions, co-first authors

Running title: Neuro-inflammation intersects with neuro-mechanobiology.

Keywords: Piezo1, neuro-inflammation, neuro-mechanobiology, focal seizures, astrocytes, microglia, pericytes, TNFα, IL1β, NF-kB.

Number of text pages: 36
Number of words: 4717
Number of Figures: 6
Number of Supplemental Figures: 3
Number of Tables: 1
Number of Supplemental Movies: 6

Corresponding Author:
Dr. Nicola Marchi, Cerebrovascular and Glia Research, Institut de Génomique Fonctionnelle (University of Montpellier, CNRS, INSERM), 141 rue de la Cardonille, 34094 Montpellier, Cedex 5, France. Email: nicola.marchi@igf.cnrs.fr.

Acknowledgment: This work was supported by ANR-EpiNeurAge, ANR-CEST-Focus, ANR/Era-Net Neu-Vasc to NM, and ANR-EpiCatcher to EB and NM. We thank Antoine dePaulis for his insightful comments and help. We are grateful to the DRCI and CRB at CHUGA.

ORCID Nicola Marchi: https://orcid.org/0000-0001-9124-0226

Abstract

Mechanosensors are emerging players responding to hemodynamic and physical inputs. Their significance in the central nervous system remains relatively uncharted. Using human-derived brain specimens or cells and a pre-clinical model of mesio-temporal lobe epilepsy (MTLE), we examined how the mRNA levels of the mechanosensitive channel PIEZO1 adjust to disease-associated pro-inflammatory trajectories.

In brain tissue micro-punches obtained from 18 drug-resistant MTLE patients, *PIEZO1* expression positively correlated with that of the pro-inflammatory biomarkers *TNFα*, *IL-1β*, and *NF-kB* in the epileptogenic hippocampus compared to the adjacent amygdala and temporal cortex. Using an experimental mouse model of MTLE, we found hippocampal *Piezo1* and cytokine expression levels increased post-status epilepticus (SE) and during epileptogenesis. *Piezo1* expression positively correlated with *Tnfα*, *Il1β*, and *Nf-kb* expression in the hippocampal foci. Next, by combining RNAscope with immunofluorescence, we identified *Piezo1* in glio-vascular cells. Post-SE and during epileptogenesis, ameboid IBA1 microglia, hypertrophic GFAP astrocytes, and damaged NG2DsRed pericytes exhibited time-dependent patterns of increased *Piezo1* expression. Digital droplet PCR analysis confirmed the *Piezo1* trajectory in isolated hippocampal microvessels in the ipsi and contralateral hippocampi. The examinations performed in this model showed *Piezo1* expression returning toward basal levels after the epileptogenesis-associated peak inflammation. From these associations, we next asked whether pro-inflammatory players directly regulate *PIEZO1* expression. We used human-derived brain cells and confirmed that

endothelium, astrocytes, and pericytes expressed *PIEZO1*. Exposure to human recombinant TNFα or IL1β upregulated *NF-kB* in all cells. Furthermore, TNFα induced *PIEZO1* expression in a dose and time-dependent manner, primarily in astrocytes.

This exploratory study describes a spatiotemporal dialogue between PIEZO1 neuro-mechanobiology and neuro-inflammatory cell remodeling. The precise cellular and functional mechanisms regulating this interplay in disease conditions warrant further investigation.

Highlights

Spatiotemporal neuroinflammatory changes correlate with PIEZO1 mRNA levels in human and rodent brains.

Glio-vascular cells present varying trajectories of *Piezo1* expression, specifically during post-SE and epileptogenesis-associated inflammation.

TNFα induces *PIEZO1* expression in human astrocytes.

These events describe a possible interplay between neuro-mechanobiology and neuroinflammation.

Introduction

Glio-vascular cells activate during brain diseases to produce inflammatory changes with precise trajectories. Within this context, glial cells modify their shape, reflecting diverse reactivity stages, and microcapillaries undergo damage and aberrant angiogenesis with deregulated blood flow dynamics (Iadecola et al., 2023; van Vliet and Marchi, 2022; Vezzani et al., 2022). These multi-cellular adjustments involve physical interactions, delineating a novel framework of neuro-mechanobiology (Tyler, 2012). Mechanosensitive ion channels at the plasma membrane, such as PIEZO1, play a key role in this process. In response to extracellular mechanical forces elicited by cell morphological changes and movement, PIEZO1 opens, activating intracellular signaling cascades driven by Ca^{++} influx (Andolfo et al., 2013). In this respect, PIEZO1 confers mechanosensitivity to endothelial cells, allowing them to respond to mechanical inputs generated by blood flow (Li et al., 2014). A mechanobiological implication of PIEZO1 has been demonstrated during tissue regeneration, arteriosclerosis (Shinge et al., 2022), osteoarthritis (Liu et al., 2022), and wound repair (Atcha et al., 2021; Lee et al., 2021), all intersecting with dysregulated homeostatic inflammation control (Liu et al., 2022).

Emerging research has begun to elucidate the expression and role of PIEZO1 in the brain. For example, in the retinal vasculature, PIEZO1 regulates blood flow (Harraz et al., 2022). The mechanical significance of PIEZO1 has also been proposed in microglial cells (Ge et al., 2023). Modulating *Piezo1* expression in an experimental model of Alzheimer's disease impacted amyloid pathology and cognitive decline (Hu et al., 2023; Jantti et al., 2022). Furthermore, *Piezo1* regulates

oligodendrocyte-mediated myelination (Yang et al., 2022) and has been demonstrated to be downregulated in multiple sclerosis (Velasco-Estevez et al., 2022). *Piezo1* also plays a role in the pathology of intracerebral hemorrhage by regulating the cellular responses to compression (Zhang et al., 2022).

Despite this important evidence, the link between neuroinflammation and PIEZO1 in the brain has only been partially explored. This knowledge gap is significant because the cellular response and relocation during disease-associated neuroinflammation generate mechanical forces (Liu et al., 2022; Turovsky et al., 2020), the latter potentially contributing to the pathology. Here, by combining molecular biology and imaging techniques performed on human specimens, *in vitro* cultured cells, and an experimental model of epilepsy, we examined the multi-cellular expression patterns of PIEZO1 in health and disease and its intersection with neuroinflammation. We analyzed *PIEZO1* in brain surgical resections from patients affected by mesio-temporal lobe epilepsy (MTLE), interrogating the link to inflammation biomarkers. Next, we tracked *Piezo1* cell-specific expression in a pre-clinical model of MTLE where spatiotemporal trajectories of inflammation and scarring processes ensue (Klement et al., 2019; van Vliet and Marchi, 2022). Finally, we used human brain-derived endothelial cells, pericytes, and astrocytes to test the hypothesis that inflammatory cytokines regulate *PIEZO1* expression. Our results describe a spatiotemporal interplay between neuro-inflammatory modifications and neuro-mechanobiology, identifying TNFα as one potential regulator of PIEZO1 mRNA expression.

Material and methods.

Patient selection

We used brain tissues from patients who underwent surgery for intractable mesio-temporal lobe epilepsy (Neuropathology Department, Grenoble-Alpes University Hospital (CHUGA), Grenoble, France). The surgical specimens were removed for therapeutic reasons and after informed consent (CPP 15-RNI-03; SH and PK at CHUGA) following the Declaration of Helsinki. Each brain resection was identified, oriented, and photographed. According to pre-surgical evaluations, micro-punches (1mm^3 each) were obtained and snap-frozen from the epileptogenic hippocampus and propagating seizure regions, amygdala, uncus, and neocortex. Upon sample transfer (CHUGA to Inserm), RT-qPCR was used to analyze all samples (n = 18 patients, for a total of 51 samples). General characteristics: 12 females and 6 males; mean age at surgery 39.6±9.3 years; seizure onset age: 12.7±8.9 years; duration of epilepsy: 27±11.9 years. These patients were under varying anti-seizure medications (alone or in combination), which were administered based on clinical choices (Valproate de sodium (VPA), Lacosamide (LCS), Levetiracetam (LEV), Oxcarbazepine (OXC), Lamotrigine (LTG), Carbamazepine (CBZ), Zonisamide (ZNS), Eslicarbazepine acetate (Zebinix), Clobazam (Urbanyl), Perampanel (Fycompa), Topiramate (TMP), Primidone (Mysoline), Ethosuximide (Zarontin). Four subjects did not present with hippocampal sclerosis. See Supplemental Figure 1 for seizure parameter distributions.

Animal housing and disease model.

Animal procedures were performed according to the European Committee Council Directive 2010/63/EU and after validation by our local ethical committee and the French Ministry of Research (Apafis#10861-2018062513068565v1). Adult C57BL/6J (genotyped for NG2DsRed) male mice were housed with food and water ad libitum and maintained in a 12-hour light-dark cycle (room temperature: 22±1°C). All experiments, including euthanasia, were performed between 9 a.m. and 2 p.m. during the daily portion of the circadian rhythm. We used male mice because, in females, the estrous cycle could impact the establishment of the epileptic models. Male mice (2-3 months old) are housed in groups (3-4) before model induction. After seizure generation, individual mice are kept for one week in separate cages and monitored daily for well-being biomarkers. After this period, two mice are maintained in one cage. To induce MTLE, stereotaxic injection of 50nL of a 20mM solution of KA (1nmol; Sigma-Aldrich) was performed into the right dorsal hippocampus under deep general anesthesia (Ketamine/Xylazine in sterile 0.9% NaCl) as previously described (Boux et al., 2021; Canet et al., 2022; Klement et al., 2019; Riban et al., 2002), while sham mice received 0.9% NaCl. Buprenorphine (sub-cutaneous, 0.05 mg/Kg) is used for analgesia. After KA injection, asymmetric clonic movements of the forelimbs, head deviations, rotations, and periods of immobility occur for a few hours. These archetypical behavioral biomarkers are associated with electrographic spontaneous seizures in at least 90% of the animals within the next few weeks, as shown (Boux et al., 2021; Riban et al., 2002). All animals were individually tracked daily for well-being, including an overnight nesting test. Animals experiencing focal SE post-

injection do not build a nest, as assessed the following day; then, they enter epileptogenesis. To conform to the 3R rules, characterized samples (-80°C bank) from precedent studies were specifically used for RT-PCR analysis (n=5 hippocampi/time point). Furthermore, we generated samples to perform microvessels isolation with ddPCR and RNAscope histology from C57BL/6J (genotyped for NG2DsRed (Arango-Lievano et al., 2018), positive or negative): n = 3/time point (sham, post-SE, one week, and four weeks) and 3-4/time point respectively. For each technique, the sham consisted of intrahippocampal injection of sterile saline, with brain tissues removed between 24h and 72h after.

RT-qPCR

RNA extraction and Reverse transcription. Brain tissues from mice and humans were kept dry frozen until extraction day. Tissues were lysed within the Lysing Matrix D tube into the Fast-Prep sample preparation system (MP Biomedicals, Santa Ana, USA 6913500). Total RNA was extracted and purified using the RNeasy Plus Mini Kit (cell cultures or tissues were extracted: Qiagen #74136) or the RNeasy Micro kit (Isolated hippocampal vessels; Qiagen #74004). For cell cultures and tissues, the RNA concentration of each sample was measured with a Nanodrop 2000c spectrophotometer (Thermo Fisher Scientific, Waltham, USA), whereas for microvessels, RNA concentration and quality were measured using a 2100 Bioanalyzer Instrument (Agilent). RNAs were retrotranscribed into complementary DNA using the Transcriptor Universal cDNA Master kit (Roche, 05893151001), using either one µg of total RNA for cells lysate and tissues, and 12 ng of total RNA for microvessels. cDNAs were diluted 5-fold in RNase/DNase-free water, then analyzed by qPCR (Tissues and cells) or ddPCR (microvessels).

Quantitive PCR was performed in 384-well plates in a final volume of 5µl using SYBR Green dye detection on the LightCycler480 system (Roche-Diagnostic). The primer pairs for the genes of interest were designed using Primer 3 software; their sequences are reported in Table 1. Melting curves were checked to ensure the presence of a single PCR product. Furthermore, each plate carried serial dilutions of an RNA calibrator to generate a standard curve of the efficiency of the primers during the run. All analyzed genes showed detectable expression levels. Gene expression levels were quantified by the $2^{-\Delta\Delta Ct}$ method with GAPDH (glyceraldehyde-3-phosphate dehydrogenase) or RPL23A (Ribosomal protein L23a) as normalizing genes. Each target value is expressed as n-fold differences relative to the control group.

Isolation of hippocampal microvessels.

Vessel isolation solutions were prepared the day before experimentation: buffer 1 (B1), add 5ml of HEPES 1M to 500ml HBSS 1X; Buffer 2 (B2), add 18g of Dextran to 100ml of B1; Buffer3 (B3), add 2,5g of BSA to 250ml of B1. Solutions B2 and B3 were filtered using a 0.80 µm filtration unit. For two hippocampus, 20ml, 16ml, and 60ml of solutions B1, B2 and B3 respectively, are required. Each procedure step was carried out on ice, centrifugations were performed at 4°C, and RNAseout (1/1000; Invitrogen, Cat No. 10777-019) was added to each buffer. Each hippocampus was dissected, placed in a beaker containing 4ml of HBSS supplemented with 10mM HEPES and 1/1000 (Buffer 1), and chopped with a scalpel. Homogenization was performed using a 5ml glass-teflon dounce homogenizer with

20 back-and-forth cycles at a rotation speed of 400rpm. After vigorous shaking for 2 min, the suspension was centrifuged at 2,000g for 10min. The pellet was resuspended with 8ml of buffer 1 supplemented with 18% Dextran and shaken vigorously for 1 min before centrifugation at 4400g for 15min. The pellet was resuspended with 5ml of buffer 1 containing 1% BSA (B3 buffer), and the suspension filtered drop by drop onto a previously moistened 20µm nylon membrane. The membrane was then transferred to a beaker containing 10ml of B3 and shaken vigorously to release the vessels. Finally, the suspension was centrifuged at 3000g for 10min, and the pellet resuspended with 1ml of buffer B1. After a last resuspension/centrifugation step at 3000g for 10min, the pellet was resuspended in 350µl of RLT Lysis Buffer and stored at -80°C until use.

ddPCR

Differential *Piezo1* expression levels were measured using droplet digital PCR (ddPCR) supermix for Probes (No dUTP) (Bio-Rad) according to the manufacturer's instructions. Detection probes and primers for *Piezo1* and *Tmed-10* (reference gene) were designed with Primer3 (Table 1). Briefly, cDNA, probes, or primers were distributed into 10,000–20,000 droplets using the QX200 Droplet Generator (Bio-Rad). The nucleic acids were then PCR-amplified in a thermal cycler and read (as the number of positive and negative droplets) with a QX200 Droplet Reader (Bio-Rad). Data are then processed using QuantSoft Analysis software (Bio-Rad). In each sample, relative *Piezo1* expression levels were calculated as the ratio between *Piezo1* and *Tmed10* positive droplets. Gene expression changes were then normalized to the sham condition. Data are then processed using QuantSoft Analysis

software (Biorad). *Tmed10*: (housekeeping) F_Primer: CAGGTGGATGGGAAAGATGTAG; B_Primer: GCCATGCAAGAGGAATTTATGG; Probe (Hex/BHQ1): AGGCTGTGCTGTTAAGGTTCCAGT. *Piezo1*: F_Primer: GCTTGCTAGAACTTCACG; B_Primer: CAACCCGCATGAGTAC; Probe (Fam/BHQ1): TGTCTGGGTGGCCCTGAAAGAAG.

Tissue preparation for RNAscope and histology

After induction of deep anesthesia (ketamine/xylazine), mice were transcardially perfused with 10ml cold PBS. Brains were extracted, fixed in 4% paraformaldehyde (PFA, Sigma, P6148) for 2h at room temperature (RT), and post-fixed overnight at 4°C in fresh 4% PFA. Tissues were then cryoprotected by successive immersions in PBS solutions containing increasing sucrose (Sigma, S7903) concentrations (i.e., 10%, 20%, and 30%). Tissues were transferred from one solution to the next when the brain sank, indicating equilibrium between the tissue block and the solution. Brains were included in OCT (TissueTek, #4583), flash frozen in −50°C Isopentane (Merck, #320404), and stored at −80°C for at least 24h. 20µm thick serial coronal sections were cut using a cryostat (Microm, NX70), directly mounted onto Superfrost slides, and stored at −80°C until use.

RNAscope (smFISH)

Detection of mouse *Piezo1* transcripts was performed on fixed sections using Advanced Cell Diagnostics RNAscope® Multiplex Fluorescent V2 kit. The RNAscope® probe used was Mm-*PIEZO1*-O2 (ACD, Cat No. 529091). The hybridization protocol was adapted from that of the manufacturer (ACD). Slides were

thawed at RT for 10 min, rapidly rinsed in PBS 1X, and fixed for 1h in PFA 4%. The slides were dehydrated in 50%, 70%, and 100% Ethanol for 5min each. The slides are dried in the oven (ACD, HybEz II oven) at 60°C for 1h. H_2O_2 treatment, target retrieval, protease treatment (ACD, protease III), probe hybridization, and signal amplification were performed according to the manufacturer's instructions. Opal 690 (Perkin Elmer; 1/500 in TSA buffer) was used to detect *Piezo1* RNAscope® probe. smFISH was followed by histological staining with GFAP to label astrocytes, IBA1 to label microglia, and NG2Dsred to label pericytes. Following incubation for 1h in PBS containing 2% horse serum and 0,2% Triton X-100 to permeabilize and block unspecific labeling, sections were incubated for 48h at 4°C in a humidified chamber with anti-GFAP 1/500 (Abcam, Cat No. ab4674) or anti-IBA1 1/1000 (Abcam, Cat No. ab178846) or anti-RFP 1/500 (Abcam, Cat No. ab124754) primary antibodies. Sections were then washed three times in PBS and incubated for 2h at RT with the appropriate secondary antibodies anti-chicken A488 1/500 (Jackson Immuno Research, Cat No. 703-545-155) or anti-rabbit CF488A 1/1000 (Sigma, Cat No. SAB4600036-250UL) or anti-rabbit A557 1/500 (R&D systems, Cat No. NL004). Sections were washed three times for 10mins in PBS, counter-stained for DAPI, and mounted using ProLong Diamond antifade mountant (Invitrogen, P36961). Slides were imaged on an Imager Z3 microscope (Zeiss) with an AxioCam 506 6MP camera. Images were acquired with a 40X Plan Apochromat 1.4 NA oil objective; each image has 15µm thick optical sections. Imaris software was used for image and cell 3D reconstructions and quantifications. Cells were classified based on their morphology, specified in the results. For each time point and cell type, we counted the number of *Piezo1* RNAscope dots in n = 27 cells from 3-4 images obtained from 3 hippocampi. Pericytes, microglial cells, and astrocytes present varying

morphological changes and proliferation or migration patterns that are complex and highly dissimilar. Optical density measurements were initially attempted, although we finally analyzed individual cells according to their resting and activation patterns. In this manner, an operator individually selected cells, and the number of RNAscope dots in each cell was assesed.

Brain cell cultures, cytokines, and yoda exposure protocols.

Human brain microvascular endothelial cells (Sciencell, Carlsbad, USA, HBMEC #1000), human brain vascular pericytes (HBVP, ScienCell #1200), and human astrocytes-hippocampal (HA-h, Sciencell #1830) were maintained in respective appropriate media (Sciencell ECM #1001, PM #1201, AM #1801) according to the supplier guidelines. Cells were then seeded in 6-wells plates (1.5×10^5/mL), precoated with fibronectin (Sciencell #8248) for endothelial cells, or poly-L-lysine (Sciencell #0413) for pericytes and astrocytes (2µg/cm2). After 48h, media were changed with added human recombinant IL-1β/IL-1F2 (R&D systems 201-LB-005) or TNF-α (R&D systems, Minneapolis, USA, 210-TA-005) at concentrations of 0.1, 1, and 10 ng/mL or PBS control (Eurobio Scientific, Les Ulis, France, CS1PBS01-01). The same protocol was applied with PIEZO1 agonist Yoda-1 (Selleck Chemicals, Houston, USA, S6678), which was used at concentrations of 0.1, 1, and 10µM, or DMSO control (Merck, Darmstadt, Germany, D2650). The cells were incubated for 4h, 16h, or 48h. Each condition was replicated in three wells. At the end of the experiment, cells were rinsed with PBS and harvested in RLT-Plus buffer (Qiagen) supplemented with 1% β-mercapto-ethanol.

Statistics

Analyses were performed using GraphPad Prism 9.5 (GraphPad Software, San Diego, USA). Data sets were processed using the Shapiro-Wilcox normality test. When normality was confirmed, we used a one-way ANOVA, otherwise a Kruskal-Wallis test. Adequate post hoc multiple comparison tests were computed. Power analysis and sample size calculations (OriginPro) are provided where appropriate (see Figure legends for details). Data are presented as mean ± standard deviation (SD). The significance threshold was set at $p < 0.05$.

Results

PIEZO1 positively correlates with changes in the expression of pro-inflammatory cytokines in human MTLE brain tissues.

We first explored whether *PIEZO1* is expressed in the pathological human brain and whether this correlates with the expression of neuroinflammatory markers. To this end, we analyzed post-surgical hippocampal foci (epileptogenic zone), the associated amygdala, and temporal cortex obtained from n = 18 drug-resistant MTLE patients (see methods for characteristics). Importantly, seizure conditions display neuroinflammatory activations (Vezzani et al., 2019). We found significantly higher *IL1β* and *TNFα* expression in the hippocampal foci compared to the associated amygdala and temporal cortex (Fig. 1A-A1). *PIEZO1* was expressed in all brain regions analyzed and was positively correlated with *IL1β*, *TNFα*, and *NF-KB* in the hippocampal foci (Fig. 1B-B2) compared to the perilesional temporal cortex (Fig. 1D-D1). In the amygdala, *PIEZO1* expression correlated with *NF-KB* (Fig. 1C2). Within this cohort of patients, we found no association between *PIEZO1* expression and the history of disease duration or seizures (Supplemental Fig. 1A-D). Unfortunately, the time to last seizures before surgery data was unavailable. Our cohort included only two patients with hippocampal sclerosis grade 2, impeding a meaningful statistical

sub-group analysis. Supplemental Fig. 3 illustrates where RT-PCR read-outs sit for these two samples compared to the rest of the cohort. These results suggest a possible interplay between neuroinflammation and *PIEZO1* expression in the epileptogenic zone.

Piezo1 expression varies temporally and regionally during epileptogenesis-associated inflammation in an MTLE model.

The analysis of human brain samples provided a late-stage snapshot of chronic disease. To understand how *Piezo1* expression varies temporally and regionally as seizures and the neuro-inflammatory process unfold, we employed an MTLE model in the mouse. We used an established preparation where the initial focal non-convulsive status epilepticus (SE) leads to focal epileptogenesis and chronic spontaneous seizures with propagating regions (Pernot et al., 2011). When probing pro-inflammatory biomarkers, we found a significant increase in *Tnfα*, *Il1β*, and *Nf-kb* expression from 24h post-SE, with higher levels during epileptogenesis and returning to baseline according to varying trajectories in the ipsilateral hippocampus (Fig. 2A-A2). Contralaterally, these cytokines increased, although quantitatively less, 24h post-SE and returned to baseline levels at chronic stages. These data show an inflammatory activation that develops over time and regionally. In this framework, we detected an increase in *Piezo1* from 24h post-SE in the epileptogenic hippocampi compared to sham. At later time points, the expression of *Piezo1* gradually decreased (Fig. 2A3).

We next asked whether *Piezo1* expression was associated with the inflammatory process that unfolds spatiotemporally in this MTLE model. *Piezo1* correlated with pro-inflammatory cytokine expression levels in the epileptogenic zone during disease progression (Fig. 2B-B2). A positive correlation between *Piezo1* and *Tnfα* expression was present in the contralateral hippocampus, although this was weak in comparison to the epileptogenic zone (Fig. 2C). These results point to a possible association between the neuroinflammatory environment and *Piezo1* expression, quantitatively varying from epileptogenic to propagating seizure regions during epileptogenesis.

Piezo1 expression patterns in glio-vascular cells.

We next examined *Piezo1* expression at the cellular level. To this end, we combined RNAscope *Piezo1* detection with immunohistochemistry for microglia (IBA1), astrocytes (GFAP), and pericytes (NG2DsRed). In control conditions, we detected low but significant *Piezo1* expression in all cell types examined (Fig.3 and Supplemental Movies 1-3). Post-SE and during epileptogenesis, hippocampal *Piezo1* expression increased in $IBA1^+$ microglial cells and hypertrophic $GFAP^+$ astrocytes, which was associated with a loss of ramifications or amoeboid soma; in both cases, the expression returned towards baseline levels at chronic stages (Fig. 3A-B). 3D Imaris rendering (Fig. 3A1-B1 and Supplemental Movies 4-5) illustrates *Piezo1* in the nucleus and the ramifications of IBA1/DAPI or GFAP/DAPI cells. At the perivascular level, NG2DsRed pericytes display a time-dependent increase in *Piezo1* expression, specifically in pericytes presenting with hypertrophic soma and highly disorganized perivascular ramifications (Fig. 3C1-C2 and Supplemental Movie 6).

Combining endothelial staining with *Piezo1* RNAscope was technically unfeasible. Using IsoB4 as an alternative did not yield conclusive results because of the simultaneous microglial staining during epileptogenesis (*not shown*). To circumvent this problem, we combined an optimized protocol for microvessel isolation with ddPCR to quantify *Piezo1* (Fig. 4A). Using this approach, we obtained CD31+ endothelial cells and CD13+ pericyte enrichment, which was confirmed by ddPCR. In parallel, as expected, neuronal and glial cell markers were reduced in these samples (Fig. 4B). Next, *Piezo1* expression was quantified in isolated hippocampal microvessels from sham, post-SE, and during epileptogenesis. *Piezo1* was detected (Fig. 4C), and its expression increased post-SE in microvessels from the ipsilateral hippocampi and, although quantitatively less, in the contralateral seizure propagating region. *Piezo1* expression returned to baseline over time (Fig. 4D). Overall, these results obtained in the experimental model demonstrate that *Piezo1* is expressed across multiple cells of the glio-vascular unit, unveiling temporal dynamics associated with the inflammatory stage of each parenchymal cell type.

Pro-inflammatory TNFα modulates PIEZO1 expression in human-derived glio-vascular cells.

Lastly, we tested the hypothesis that specific pro-inflammatory cytokines can induce *PIEZO1* expression. To this end, we initially determined *PIEZO1* in cultured human glio-vascular cells. In this manner, we were able to detect *PIEZO1* in multiple cell types (mean ± SD normalized to *GAPDH* expression; endothelial cells: 0,0002735 ± 0,001209; pericytes: 0,0003576 ± 0,0001195; astrocytes: 0,0002385 ±

0,0001991). Next, human recombinant IL1β or TNFα were added to the cell cultures, which elicited an increase in *NF-KB* expression indicative of an inflammatory response (Fig. 5A-C and 6A-C). This effect was more pronounced following treatment. Under these conditions, TNFα treatment increased *PIEZO1* expression in a cell, time (4h, 16h, 48h), and dose (0,1; 1; 10 ng/ml; see (Lee et al., 2021)) dependent manner. In particular, TNFα triggered a stable upregulation of *PIEZO1* in astrocytes (Fig. 5C1), while in endothelial cells this change was time-dependent at a specific cytokine concentration (Fig. 5B1). IL1β did not affect *PIEZO1* expression (Fig. 6A1-C1). As a corollary, we also investigated whether PIEZO1 activation, using a specific agonist Yoda-1, could regulate cytokine signaling. We found that Yoda-1 exposure resulted in moderately increased *NF-kB* expression in astrocytes (Supplemental Fig. 2C) and that it could also modulate *NF-kB* expression in endothelial cells depending on exposure time (Supplemental Fig. 2B). The overall effects of Yoda-1 were significantly lower compared to cytokine treatments. Yoda-1 exposure did not modify *PIEZO1* expression (Supplemental Fig. 2A1-C1). Next, we compiled all the *NF-kB* data obtained with the highest doses of TNFα, IL1β, and Yoda-1 and asked whether an inflammation threshold could control *PIEZO1* mRNA levels. Using this approach, we found a TNFα-dependent increase in *NF-kB* expression corresponded to the highest *PIEZO1* expression levels in astrocytes (Supplemental Fig. 1E). These results unveil a specific functional effect of TNFα in modulating *PIEZO1* levels. The exact signaling mechanism remains to be elucidated.

Discussion

Mechanosensors such as PIEZO1 have been demonstrated to play crucial roles in cell adaptation to mechanical forces (Coste et al., 2010; Emig et al., 2021; Harraz et al., 2022; Tyler, 2012). Despite these inroads, little is known about the role of mechanosensing in brain diseases. Here, we provide initial evidence that *PIEZO1* expression is regionally correlated with pro-inflammatory cytokines in human epileptogenic tissues. From this observation, we outlined the multi-cellular distribution of *Piezo1* in healthy and experimental MTLE hippocampi during epileptogenesis and when inflammation unfolds and resolves. Finally, we showed that TNFα can induce *PIEZO1* expression in human-derived glio-vascular cells. Our exploratory study describes the interplay between neuro-inflammation and neuro-mechanobiology in a brain disease setting and uncovers the interaction between TNFα signaling and PIEZO1 expression.

Neuro-inflammation and neuro-mechanobiology: the chicken or the egg?

In brain disease, glio-vascular cells react and relocate in a time-dependent manner. Reactive astrocytes and microglial cells undergo morphological changes,

and at the microcapillary level, pericytes remodel with pro-angiogenic adjustments. This multi-cellular reorganization is associated with inflammation and provokes biomechanical and shear microenvironmental forces (Hladky and Barrand, 2014; Liu et al., 2022; Saotome et al., 2018). Our data indicate that *PIEZO1* expression positively correlates with *TNFα*, *IL1β*, and *NF-kB* expression in human hippocampal samples (Fig.1). *PIEZO1* expression levels were similar across sub-regions tested in the human tissues (Supplemental Fig. 2A); the significant correlations in the hippocampus could be a late imprint of an antecedent inflammatory trajectory, perhaps characteristic of the epileptogenic zone. *In vivo*, the epileptogenic zone presented the most significant changes, with the seizure-propagating contralateral hippocampus temporally participating in the network pathology (Fig. 2 and 4). The latter results are coherent with our previous data indicating transient or time-dependent molecular fingerprints in seizure-propagating regions in this model (Boux et al., 2021; Canet et al., 2022). We report that *Piezo1* expression levels return towards baseline over time, indicating dynamic changes during epileptogenesis. However, the time-specific correlations between the number of seizures and *Piezo1* or cytokine expression during experimental MTLE progression must be assessed. Finally, we report that *PIEZO1* expression increased upon TNFα exposure *in vitro*, along with maximal *NF-kB* induction (Fig. 5 and Supplemental Fig. 1E). The exact intracellular mechanism by which TNFα modulates *PIEZO1* expression requires further investigation (Liu et al., 2017).

Brain Piezo1 in health and pathological trajectories.

PIEZO1 mRNA was detected in the brain at a multi-cellular level. From these results, we hypothesize a disease-related intersection between mechanical input and glio-vascular remodeling. An inflammatory scar develops in this MTLE model, specifically in the epileptogenic hippocampi (Klement et al., 2019), possibly impacting tissue mechanical properties and PIEZO1 activity. Importantly, mechanical cell activation can be beneficial, as in tissue regeneration (Harraz et al., 2022; Li et al., 2014). Therefore, the variations and modulation of PIEZO1 expression during disease development, from acute to chronic stages, could have different, perhaps contrasting, effects depending on the inflammatory landscape and its cell-specificity. For instance, in models of Alzheimer's disease (AD) and multiple sclerosis (MS), PIEZO1 modulation leads to opposite effects. In AD, microglia lacking *Piezo1* exacerbates Aβ pathology and cognitive decline, and pharmacological activation of PIEZO1 in microglial enhances phagocytosis and Aβ clearance (Hu et al., 2023; Jantti et al., 2022; Lewis, 2023). On the other hand, in MS, activation of PIEZO1 in oligodendrocytes inhibits proliferation and migration while, in axons, it negatively regulates myelination (Velasco-Estevez et al., 2022; Yang et al., 2022). PIEZO1 inhibition in CD4+ T cells or T regulatory cells reduces experimental autoimmune encephalitis symptoms (Yang et al., 2022). This disease-specific divergence can be attributed to the cell type involved during the pathological steps from early to chronic stages. In particular, glio-vascular cells can acquire pro-inflammatory and anti-inflammatory phenotypes temporally and regionally contingent on their redistributions around lesions (Streit et al., 2020). We hypothesize that modulation of PIEZO1 in glio-vascular cells could lead to different outcomes depending on their activation state.

In astrocytes, PIEZO1-mediated mechanotransduction regulates neurogenesis and cognitive functions (Chi et al., 2022; Turovsky et al., 2020). LPS-stimulated astrocytes exposed to a PIEZO1 activator display a reduced inflammatory phenotype (Velasco-Estevez et al., 2020). Interestingly, peripheral macrophages devoid of PIEZO1 show reduced inflammation and improved wound-healing responses (Atcha et al., 2021; Lee et al., 2021; Liu et al., 2022; Shinge et al., 2022). Furthermore, increased *Piezo1* expression in chondrocytes is associated with a feed-forward pathological mechanism, with excess intracellular Ca^{2+} and F-actin cytoskeleton rarefication (Lee et al., 2021). This evidence indicates that increased PIEZO1 activity or expression favors inflammatory reactions; within this framework, our data highlight a correlation between pro-inflammatory *TNFα* and *PIEZO1* expression, perhaps particularly relevant to astrocytes. Astrocytes play a critical role in regulating brain architecture, so their physical properties are crucial. Recent evidence indicates that PIEZO1 plays a role in regulating cell stiffness in pathological situations. Recent research suggests that increased PIEZO1 expression in human atrial fibroblasts increases cell stiffness due to changes in cytoskeletal architecture (Emig et al., 2021). Recent advances indicate that brain tonometry may aid neurosurgeons in identifying abnormal brain tissue during epilepsy surgery (Fallah et al., 2020). It is, therefore, possible that PIEZO1 could mediate increased astrocyte-associated brain stiffness in response to seizure-induced neuroinflammation. The latter could also involve blood-brain barrier damage and alterations in interstitial fluid clearance. Future studies targeting PIEZO1, specifically in glial cells, will be required to determine if this is the case (Turovsky et al., 2020).

Limitations, Perspective, and Conclusions.

Our exploratory study presents limitations and opportunities for further research. For instance: i) increasing the number of samples is necessary to fully meet power analysis criteria; ii) we combined RNAscope and immunofluorescence using one antibody at a time for each cell type; iii) at present, we cannot determine whether the changes in *Piezo1* expression we have observed correlate with changes in functional protein levels. The latter would require detailed electrophysiology of individual cell types, which is beyond the capacity of this current research. A previous study assessing the role of PIEZO1 in glioblastomas demonstrated a correlation between increasing levels of mRNA and protein (Chen et al., 2018); iv) a comprehensive investigation needs to be performed to understand the impact of HS severity and grading; v) other cytokines and mechanosensors could be involved; vi) we did not test primary human microglial cells as their cell culture requires specific differentiation protocols and cultivation with neurons to obtain microglia-like derived cells (Takata et al., 2017), exceeding the capacity of our study. Nevertheless*, in vivo*, we report that morphologically reactive microglial cells display increased *Piezo1* expression; vii) we recognize the need for experiments exploring the functional consequences of PIEZO1 regulation in an epilepsy model. Pharmacological or genetic manipulations of PIEZO1 should be performed to study whether its activation or blockade could modify seizure-associated pathology over time; viii) the exact intracellular signaling tying cytokines to PIEZO1 expression and function needs to be outlined; ix) from a technical standpoint, the detection levels of the housekeeping genes did not significantly change in human and mouse tissues (*not shown*). This result is coherent with the stability of GAPDH in models of brain disorders, including seizures (Aithal and Rajeswari, 2015; Bruckert et al., 2016; Marques et al., 2013;

Schwarz et al., 2020). We recognize that the available clinical dataset did not allow us to perform focused correlations between HS grading, pathology, and these housekeeping genes; x) mechanical isolation of microvessels can activate the cells; here, a sham microvessel group was used to account for this possible caveat. This caution generally applies to cell isolation from a complex tissue.

In summary, these data indicate that neuro-mechanobiology and neuro-inflammation are intertwined according to spatiotemporal trajectories. Modulating the transduction of inflammatory and mechanical signals could unveil novel aspects of brain disease progression.

Declarations of interest: NONE.

Use of AI or ChatGPT: NONE.

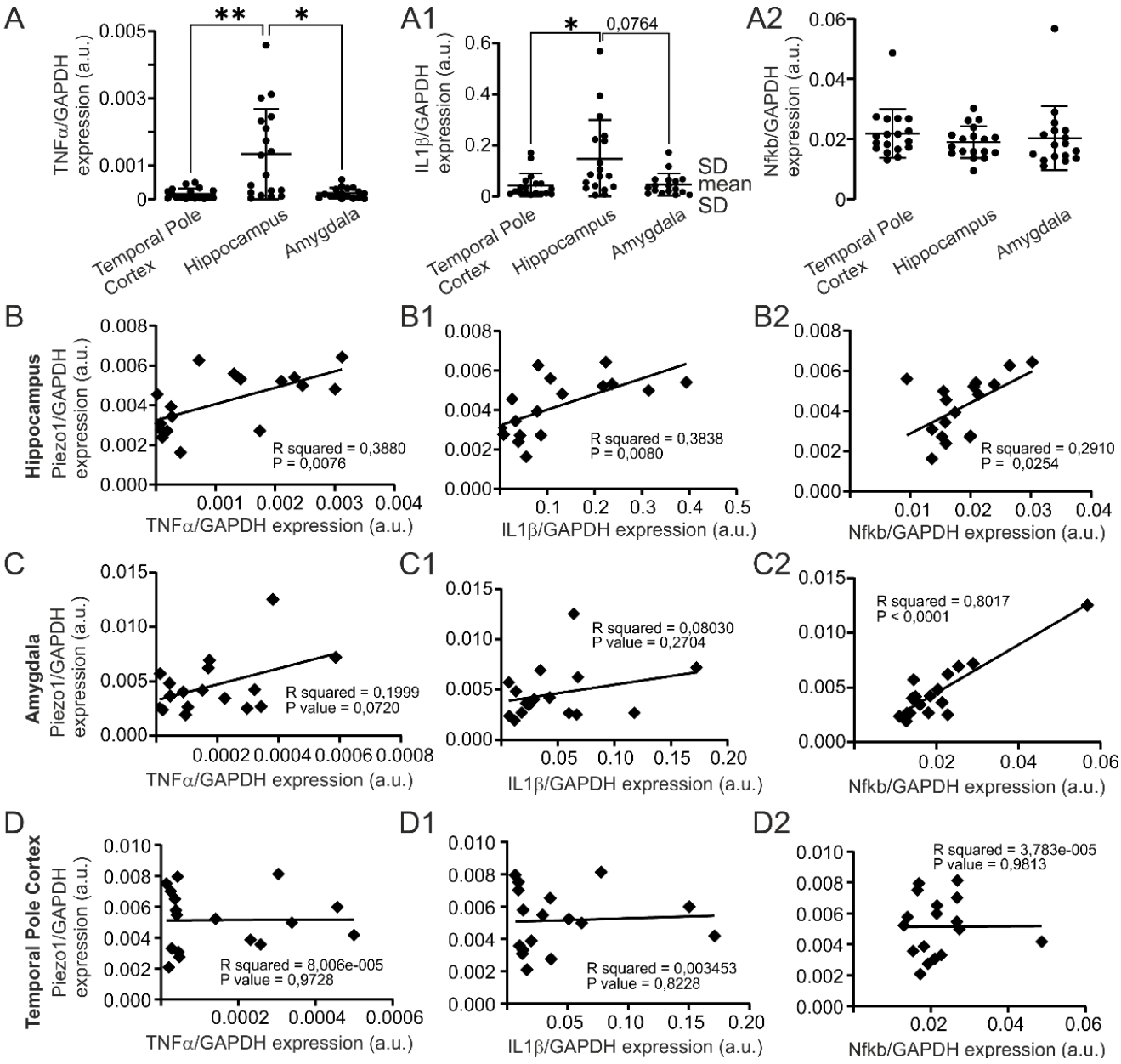

Figure 1. Linear correlations between pro-inflammatory cytokines and *PIEZO1* levels in human TLE. A-A2) RT-qPCR quantifications for *TNFα*, *IL1β*, and *NF-kB* in three sub-regions (epileptogenic hippocampus, perilesional cortex, and amygdala micro-punches) obtained from each resected TLE tissue. **B-B2)** Correlations, or lack thereof, between *PIEZO1* and cytokines in the hippocampi, **C-C2)** amygdala, and **D-D2)** temporal cortex**.** Each data point indicates a single micro-punch brain sample from n = 18 patients (arbitrary units normalized by housekeeping gene *GAPDH*; mean ± SD). Kruskal-Wallis and Dunn's post hoc for multiple comparisons and Spearman test for correlation were performed.

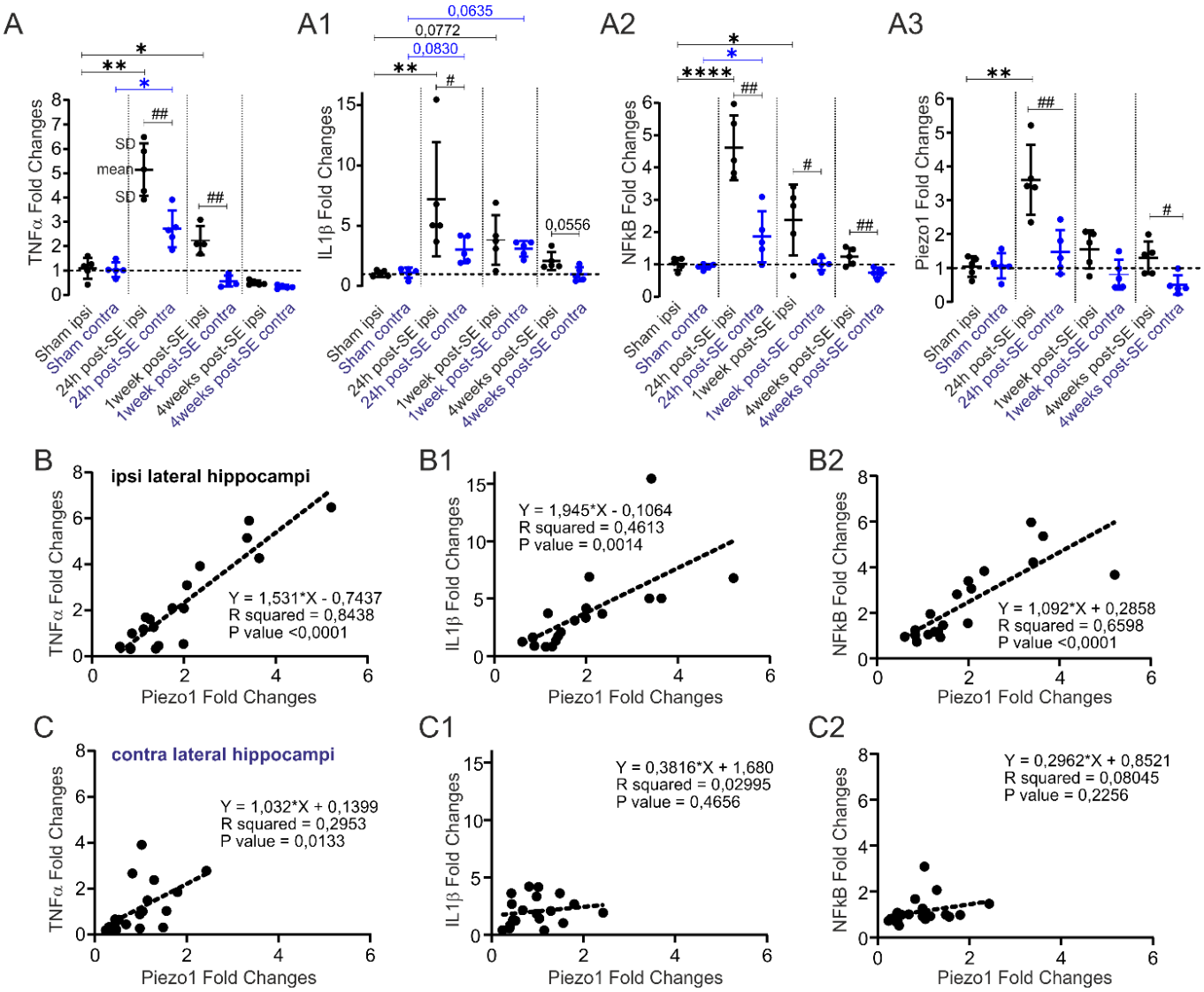

Figure 2. Spatiotemporal *Piezo1* expression in a TLE model is associated with hippocampal neuroinflammatory dynamics. A-A3) Patterns of *Tnfα*, *Il1β*, *Nf-kb*, and *Piezo1* overexpression post-SE and during epileptogenesis in the ipsilateral epileptogenic and the contralateral seizure propagating zone. **B-B2)** Linear correlations, or lack thereof, between *Piezo1* expression and cytokine levels, measured over time in the ipsilateral epileptogenic and **(C-C2)** contralateral seizure propagating hippocampi. Each data point corresponds to one hippocampus, n = 5 for each time point. Data are indicated as fold change compared to sham normalized by *Gapdh* (mean ± SD). One-way ANOVA and Tukey's post hoc for multiple comparisons; Mann-Whitney test was used for ipsilateral and contralateral comparisons. Pearson coefficients for correlations were performed. Actual power and sample size calculations for sham vs experimental group comparisons, excluding cases where power is already > 0.8 and no changes: Piezo1 ipsilateral hippocampi Sham vs. 1week, actual power = 0.34 (n = 15 + 15 for a power > 0.8); Il1b ipsilateral hippocampi Sham vs. 24h, actual power = 0.72 (n = 6 + 6 for a power > 0.8); Il1b ipsilateral hippocampi Sham vs. 1week, actual power = 0.75 (n = 6 + 6 for a power > 0.8); Nf-kb ipsilateral hippocampi Sham vs. 1week, actual power = 0.66 (n 7 + 7 for power > 0.8); Tnfα contralateral hippocampi Sham vs. 1week, actual power = 0.73 (n = 6 + 6 for a power > 0.8)".

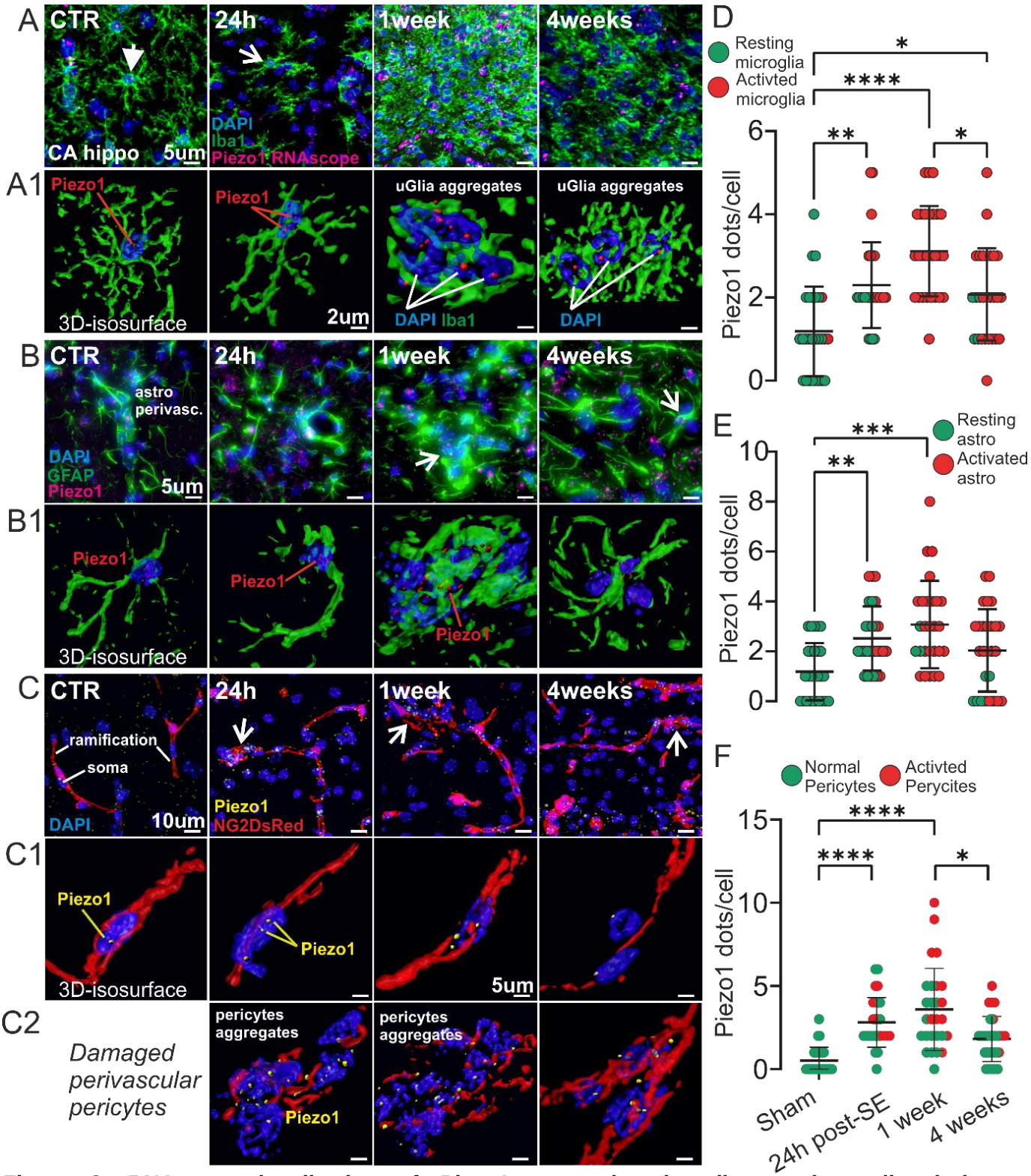

Figure 3. RNAscope localization of *Piezo1* expression in glio-vascular cells during epileptogenesis and pro-inflammatory activations. A) Examples of *Piezo1* RNA localization at IBA1^{+} microglial cells, **(B)** GFAP^{+} astrocytes, and **(C)** NG2DsRed^{+} pericytes in control, post-SE, epileptogenesis (1 week) and spontaneous seizures (4 weeks) in the epileptogenic hippocampus. **A1-**

B1-C1-C2) Examples of Imaris 3D cellular isosurface rendering to illustrate *Piezo1* expression in the $DAPI^+$ nuclei and various cellular ramifications. See Supplemental Movies 1-6 for 3D details. **D-F)** Cellular activation or damage 24h post-SE and at one week corresponded to peak *Piezo1* expression. Each data point corresponds to one cell (27 cells from 3-4 images and 3 mice/time point). Kruskal-Wallis and Dunn's post hoc test for multiple comparisons was performed. Power is > 0.8 for statistically significant results.

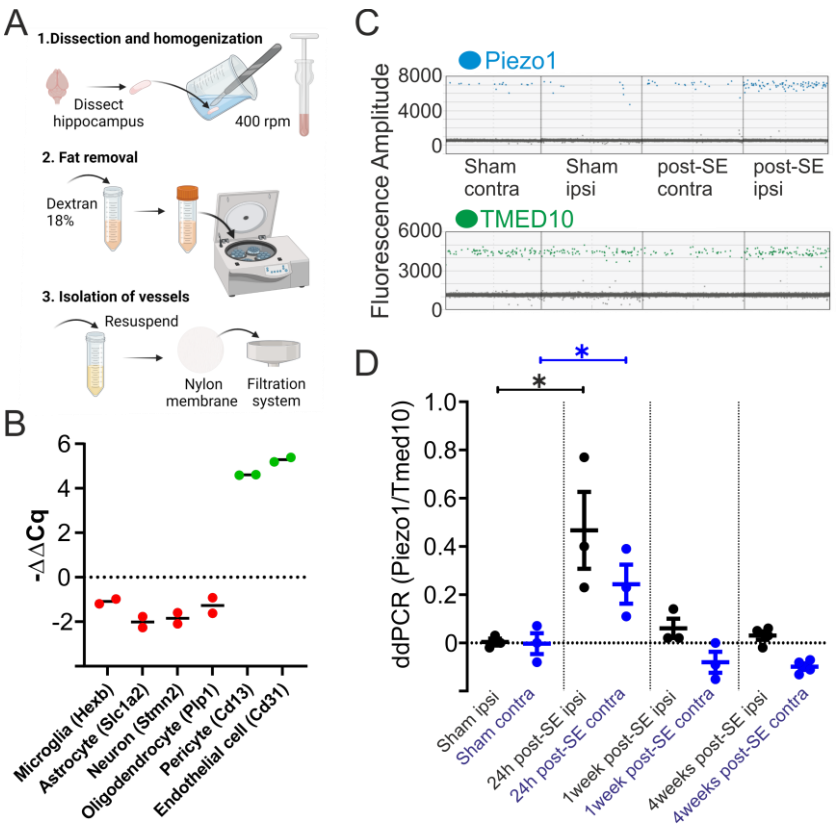

Figure 4. Pattern of *Piezo1* expression during epileptogenesis at isolated hippocampal microvessels. A) Schematic representation of methods. **B)** Quality control for *Cd31* and *Cd13* enrichment (housekeeping gene *Tmed10*). **C)** Examples of ddPCR reading for *Piezo1* and reference *Tmed10*. **D)** *Piezo1* microvascular overexpression (normalized by *Tmed10* and as compared to sham) post-SE returning to sham values over time in ipsilateral and contralateral hippocampi. Normality was tested using Shapiro-Wilk. One-way ANOVA and Holm-Sidak's post hoc (contralateral) or Kruskal-Wallis and Dunn's multiple comparisons (ipsilateral) were performed. Piezo1 ipsilateral hippocampi Sham vs. 24h, actual power = 0.59 (n = 4 + 4 for a power > 0.8); Piezo1 contralateral hippocampi Sham vs. 24h, actual power = 0.53 (n = 5 + 5 for a power > 0.8)

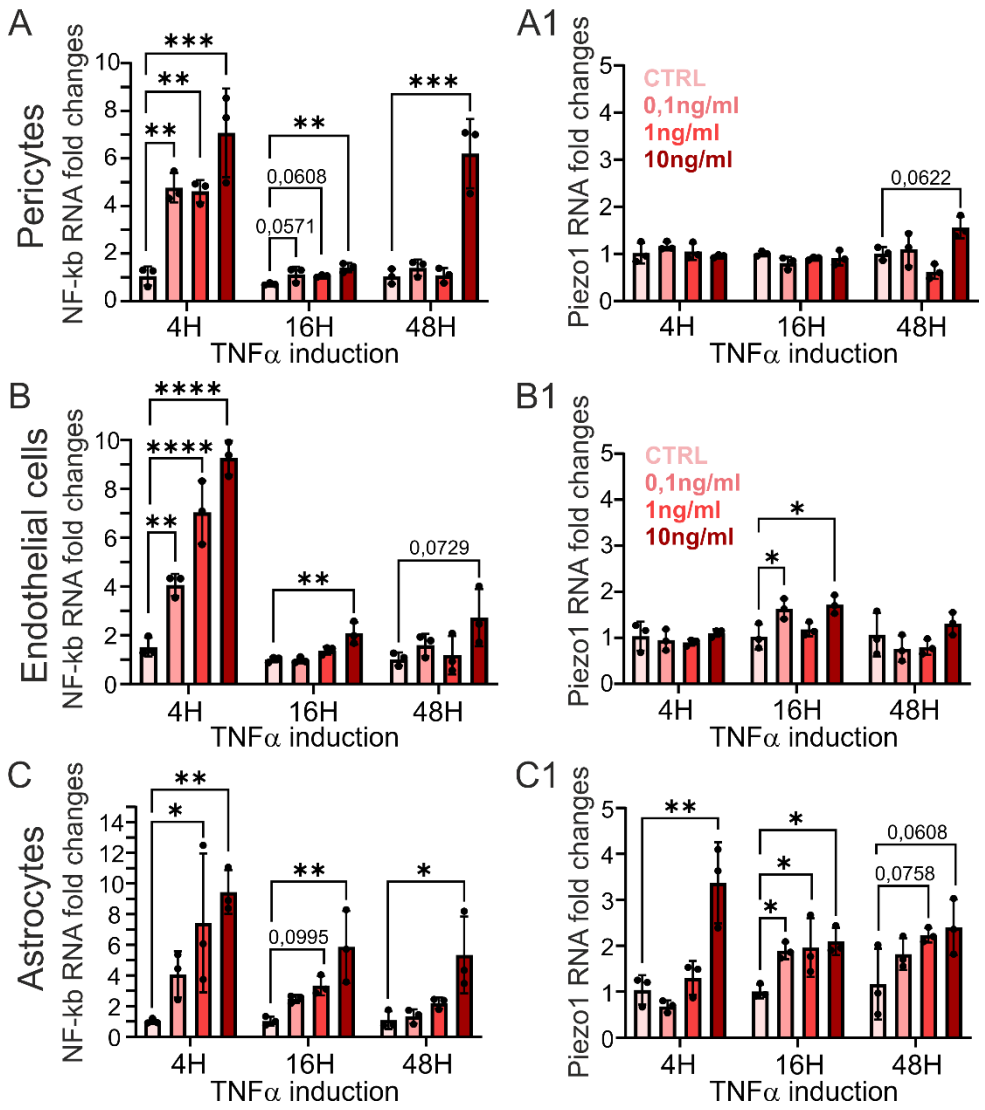

Figure 5. TNFα exposure upregulates *PIEZO1* expression preferentially in human-derived brain astrocytes. A-C) TNFα time and dose-dependent inflammatory (*NF-kB)* activation in pericytes, endothelial cells, and astrocytes. **A1-C1)** In response to TNFα, *PIEZO1* is overexpressed in astrocytes compared to endothelial cells and pericytes. Data points correspond to culture wells (n = 3) for each dose and time point. Experiments were run separately for 4h, 16h, and 48h. Data are indicated as fold change compared to sham and normalized with housekeeping genes *GAPDH* and *RPL23A* (mean ± SD). Normality was tested using Shapiro-Wilk. One-way ANOVA and Holm-Sidak's post hoc or Kruskal-Wallis and Dunn's multiple comparisons were performed.

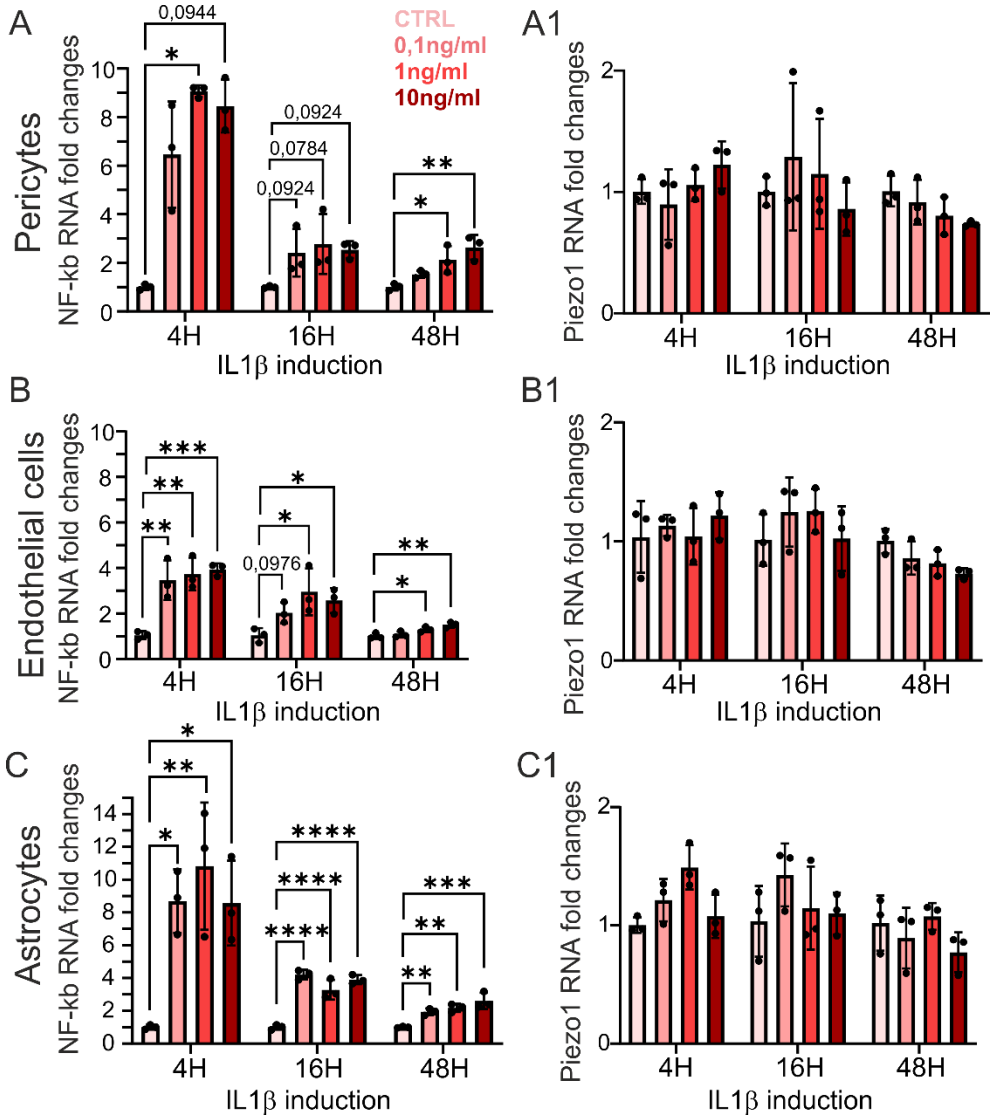

Figure 6. IL-1β exposure does not cause *PIEZO1* up-regulation in human-derived glio-vascular cells. A-C) IL1β time and dose-dependent inflammatory (*NF-kB)* activation in pericytes, endothelial cells, and astrocytes. *NF-kB* variations over time are dissimilar between IL1β and TNFα (see Figure 5) stimulations. **A1-C1)** Exposure to IL1β did not modify *PIEZO1* expression. Data points correspond to culture wells (n = 3) for each dose and time point. Experiments were run separately for 4h, 16h, and 48h. Data are indicated as fold change compared to sham and normalized with housekeeping genes *GAPDH* and *RPL23A* (mean ± SD). Normality was tested using Shapiro-Wilk. One-way ANOVA and Holm-Sidak's post hoc or Kruskal-Wallis and Dunn's multiple comparisons were performed.

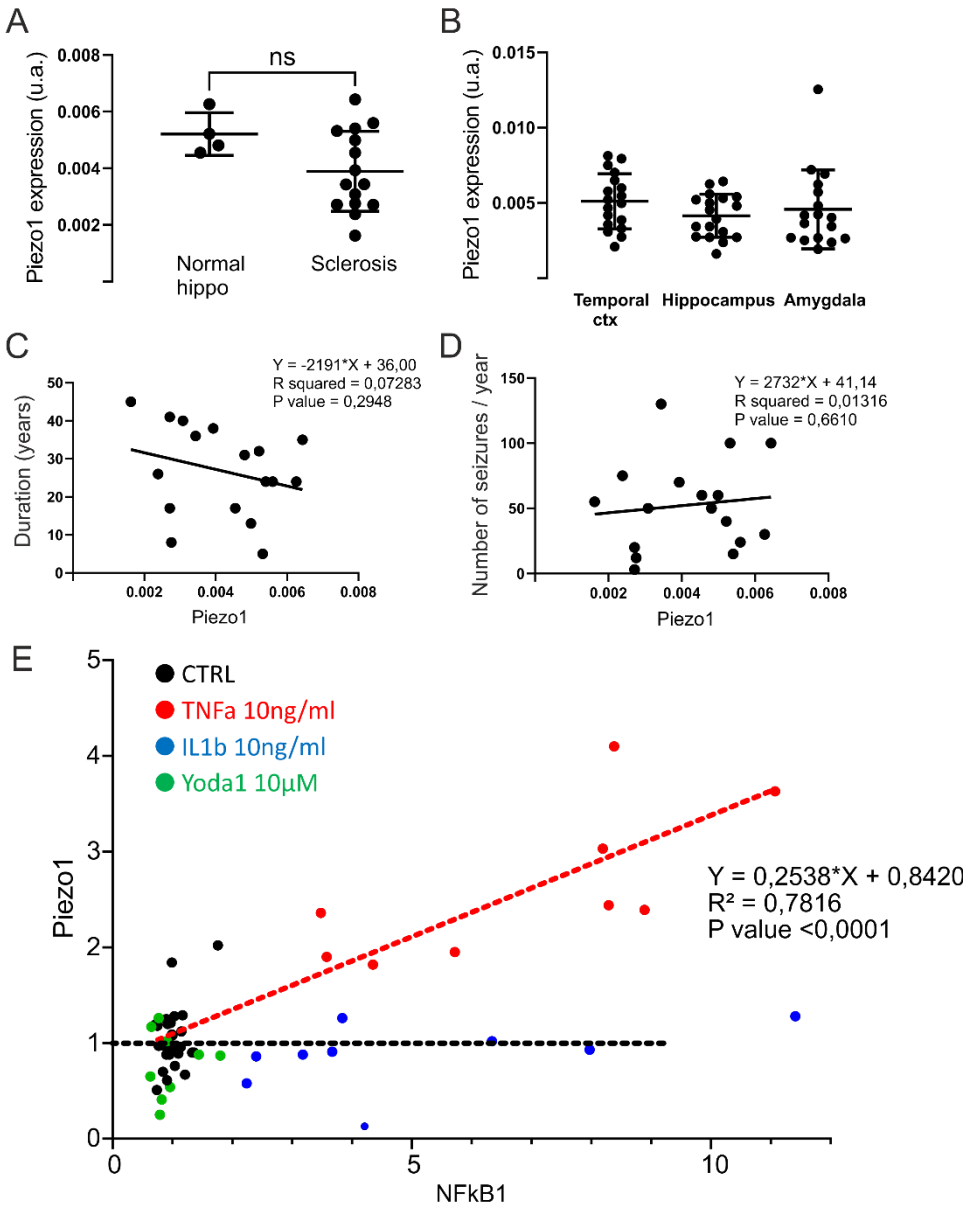

Supplemental Fig. 1. A-D) *PIEZO1* expression in human TLE tissue sub-regions and correlations with clinical parameters (normalized by *GAPDH*). Data are indicated as single micro-punch samples from n = 18 patients (mean ± SD). Unpaired t–test and Kruskal-Wallis and Spearman coefficient were computed. **E)** *PIEZO1* and *NF-kB* correlation in human-derived astrocytes across treatments. Each value corresponds to one cultured well with different molecules (linear regressions with Pearson coefficient).

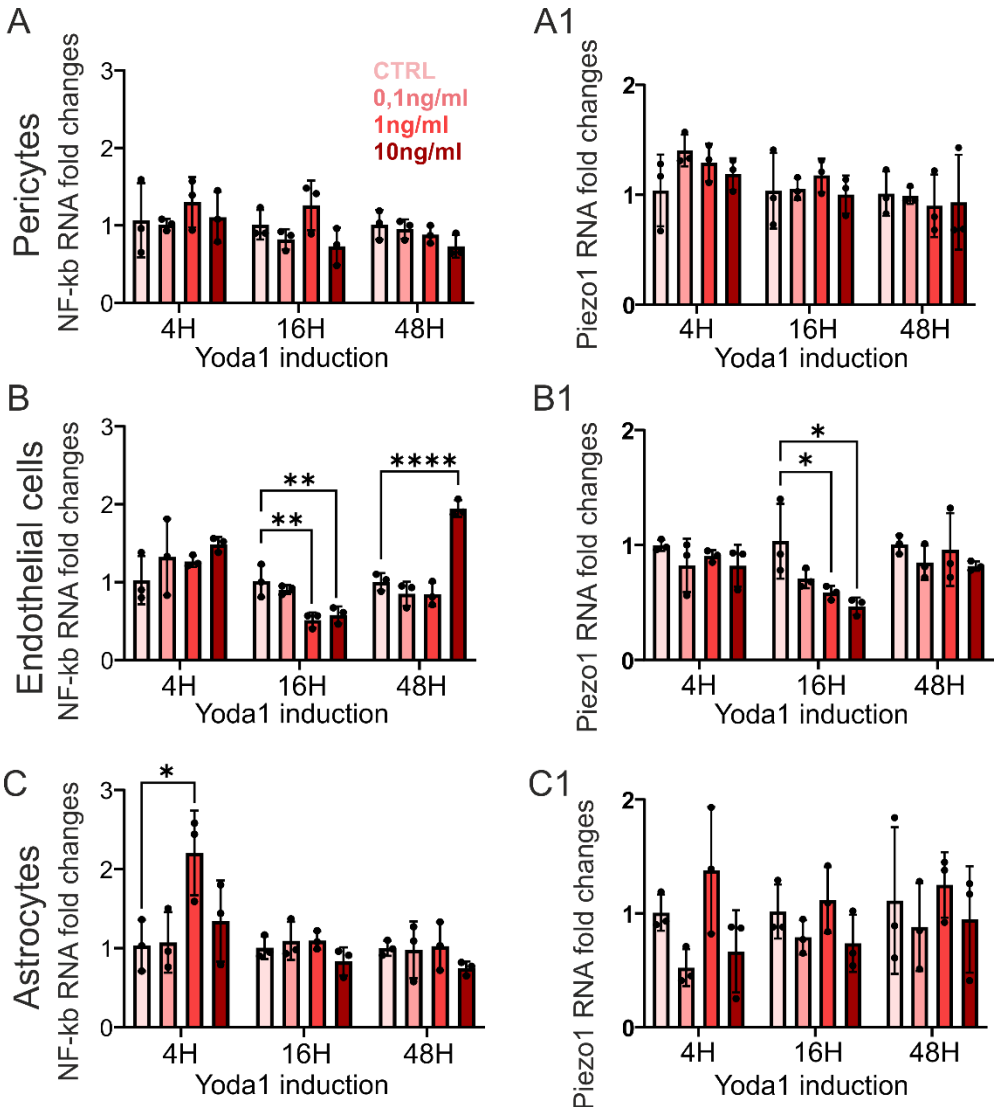

Supplemental Fig.2. Yoda1 marginally modulates *NF-kB* expression without affecting *PIEZO1* expression in human-derived glio-vascular cells. A-C) *NF-kB* levels in pericytes, endothelial cells, and astrocytes. **A1-C1)** *PIEZO1* levels in pericytes, endothelial cells, and astrocytes. Data points correspond to culture wells (n = 3) for each dose and time point. Experiments were run separately for 4h, 16h, and 48h. Data are indicated as fold change compared to sham and normalized with housekeeping genes *GAPDH* and *RPL23A* (mean ± SD). Normality was tested using Shapiro-Wilk. One-way ANOVA and Holm-Sidak's post hoc or Kruskal-Wallis and Dunn's multiple comparisons were performed.

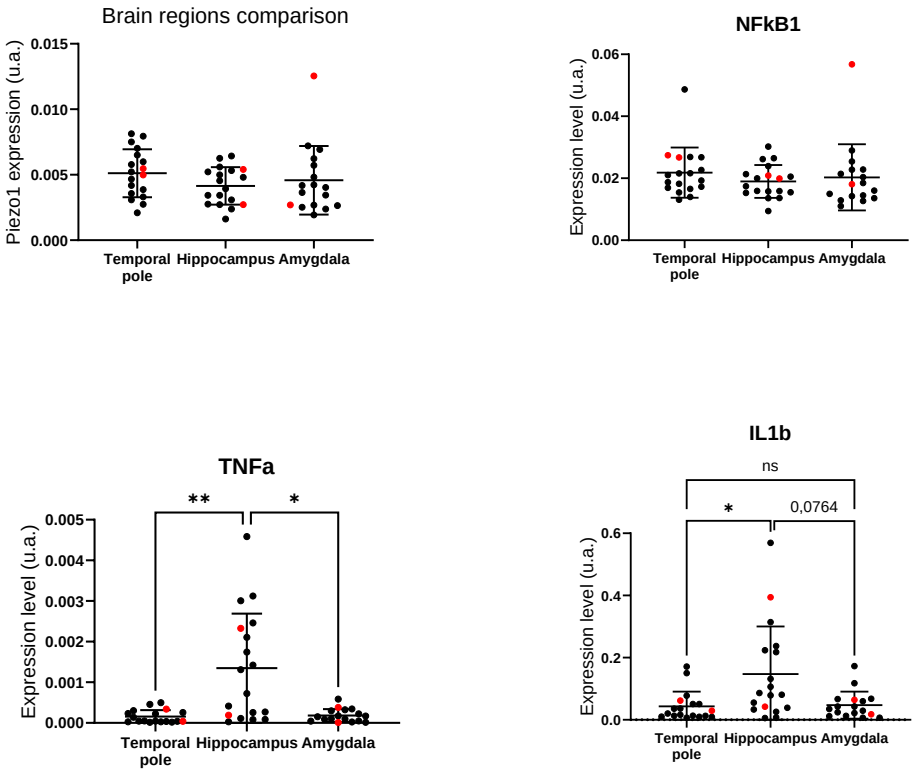

Supplemental Fig.3. Distribution of HS grade 2 samples (red) within the studied cohort. The few samples available did not allow us to determine the impact of HS severity of the read-outs examined.

Table 1. RT-qPCR primers

Gene name	**Specie**	**Forward primer (5' - 3')**	**Reverse primer (5' - 3')**	**Product length**	**Tm**
Piezo1	mouse	CTGGACCAGTTTCTGGGACAA	AGCCTGGTGGTGTTAAAGATGT	104	59,88
Nf-kb 1	mouse	CAGCTTCGGAGGAAATCAG	CCGAGAAGTTCGGCATAAG	121	55,77
Il1b	mouse	TGCCACCTTTTGACAGTGATG	AAGGTCCACGGGAAAGACAC	220	59,47
Tnfa	mouse	GCTGAGCTCAAACCCTGGTA	CCGGACTCCGCAAAGTCTAA	119	59,72
Gapdh	mouse	CTTGAAGGGTGGAGCCAAAAG	TGTGGTCATGAGCCCTTCC	199	59,35
PIEZO1	human	ACTTTCCCATCAGCACTCGG	CCACGAAGTCCTTGAGACCC	165	60,04
NF-kb 1	human	AGAGGCGTGTATAAGGGGCT	CTGCTTGGCGGATTAGCTCT	125	60,29
IL1b	human	CAGGCTGCTCTGGGATTCTC	GTCCTGGAAGGAGCACTTCAT	172	59,95
TNFa	human	TGCACTTTGGAGTGATCGGC	CAGCTTGAGGGTTTGCTACAAC	144	60,5
GAPDH	human	AAATCAAGTGGGGCGATGCT	CAAATGAGCCCCAGCCTTCT	86	60,32
RPL23A	human	AGCCTACAAGAAAGTTTGCCTAT	TCTTCTTCCGGTAGTGGATCTTGGC	126	61,09

Bibliography

Aithal, M. G., Rajeswari, N., 2015. Validation of housekeeping genes for gene expression analysis in glioblastoma using quantitative real-time polymerase chain reaction. Brain Tumor Res Treat. 3**,** 24-9.

Andolfo, I., Alper, S. L., De Franceschi, L., Auriemma, C., Russo, R., De Falco, L., Vallefuoco, F., Esposito, M. R., Vandorpe, D. H., Shmukler, B. E., Narayan, R., Montanaro, D., D'Armiento, M., Vetro, A., Limongelli, I., Zuffardi, O., Glader, B. E., Schrier, S. L., Brugnara, C., Stewart, G. W., Delaunay, J., Iolascon, A., 2013. Multiple clinical forms of dehydrated hereditary stomatocytosis arise from mutations in PIEZO1. Blood. 121**,** 3925-35, S1-12.

Arango-Lievano, M., Boussadia, B., De Terdonck, L. D. T., Gault, C., Fontanaud, P., Lafont, C., Mollard, P., Marchi, N., Jeanneteau, F., 2018. Topographic Reorganization of Cerebrovascular Mural Cells under Seizure Conditions. Cell Rep. 23**,** 1045-1059.

Atcha, H., Jairaman, A., Holt, J. R., Meli, V. S., Nagalla, R. R., Veerasubramanian, P. K., Brumm, K. T., Lim, H. E., Othy, S., Cahalan, M. D., Pathak, M. M., Liu, W. F., 2021. Mechanically activated ion channel Piezo1 modulates macrophage polarization and stiffness sensing. Nat Commun. 12**,** 3256.

Boux, F., Forbes, F., Collomb, N., Zub, E., Maziere, L., de Bock, F., Blaquiere, M., Stupar, V., Depaulis, A., Marchi, N., Barbier, E. L., 2021. Neurovascular multiparametric MRI defines epileptogenic and seizure propagation regions in experimental mesiotemporal lobe epilepsy. Epilepsia.

Bruckert, G., Vivien, D., Docagne, F., Roussel, B. D., 2016. Normalization of Reverse Transcription Quantitative PCR Data During Ageing in Distinct Cerebral Structures. Mol Neurobiol. 53**,** 1540-1550.

Canet, G., Zub, E., Zussy, C., Hernandez, C., Blaquiere, M., Garcia, V., Vitalis, M., deBock, F., Moreno-Montano, M., Audinat, E., Desrumaux, C., Planel, E., Givalois, L., Marchi, N., 2022. Seizure activity triggers tau hyperphosphorylation and amyloidogenic pathways. Epilepsia. 63**,** 919-935.

Chen, X., Wanggou, S., Bodalia, A., Zhu, M., Dong, W., Fan, J. J., Yin, W. C., Min, H. K., Hu, M., Draghici, D., Dou, W., Li, F., Coutinho, F. J., Whetstone, H., Kushida, M. M., Dirks, P. B., Song, Y., Hui, C. C., Sun, Y., Wang, L. Y., Li, X., Huang, X., 2018. A Feed-forward Mechanism Mediated by Mechanosensitive Ion Channel PIEZO1 and Tissue Mechanics Promotes Glioma Aggression. Neuron. 100**,** 799-815 e7.

Chi, S., Cui, Y., Wang, H., Jiang, J., Zhang, T., Sun, S., Zhou, Z., Zhong, Y., Xiao, B., 2022. Astrocytic Piezo1-mediated mechanotransduction determines adult neurogenesis and cognitive functions. Neuron. 110**,** 2984-2999 e8.

Coste, B., Mathur, J., Schmidt, M., Earley, T. J., Ranade, S., Petrus, M. J., Dubin, A. E., Patapoutian, A., 2010. Piezo1 and Piezo2 are essential components of distinct mechanically activated cation channels. Science. 330**,** 55-60.

Emig, R., Knodt, W., Krussig, M. J., Zgierski-Johnston, C. M., Gorka, O., Gross, O., Kohl, P., Ravens, U., Peyronnet, R., 2021. Piezo1 Channels Contribute to the Regulation of Human Atrial Fibroblast Mechanical Properties and Matrix Stiffness Sensing. Cells. 10.

Fallah, A., Subramaniam, T., Phillips, H. W., Michalet, X., Vinters, H. V., Yong, W. H., Wu, J. Y., Salamon, N., Ellingson, B. M., Wang, A. C., Reyes, S. D., Ibrahim, G. M., Weil, A. G., Chang, J. W., Babayan, D., Nguyen, J. C., Behnke, E.,

Tseng, C. H., Mathern, G. W., 2020. Novel tonometer device distinguishes brain stiffness in epilepsy surgery. Sci Rep. 10**,** 20978.
Ge, G. R., Rolland, J. P., Song, W., Nedergaard, M., Parker, K. J., 2023. Fluid compartments influence elastography of the aging mouse brain. Phys Med Biol. 68.
Harraz, O. F., Klug, N. R., Senatore, A. J., Hill-Eubanks, D. C., Nelson, M. T., 2022. Piezo1 Is a Mechanosensor Channel in Central Nervous System Capillaries. Circ Res. 130**,** 1531-1546.
Hladky, S. B., Barrand, M. A., 2014. Mechanisms of fluid movement into, through and out of the brain: evaluation of the evidence. Fluids Barriers CNS. 11**,** 26.
Hu, J., Chen, Q., Zhu, H., Hou, L., Liu, W., Yang, Q., Shen, H., Chai, G., Zhang, B., Chen, S., Cai, Z., Wu, C., Hong, F., Li, H., Chen, S., Xiao, N., Wang, Z. X., Zhang, X., Wang, B., Zhang, L., Mo, W., 2023. Microglial Piezo1 senses Abeta fibril stiffness to restrict Alzheimer's disease. Neuron. 111**,** 15-29 e8.
Iadecola, C., Smith, E. E., Anrather, J., Gu, C., Mishra, A., Misra, S., Perez-Pinzon, M. A., Shih, A. Y., Sorond, F. A., van Veluw, S. J., Wellington, C. L., American Heart Association Stroke Council Council on Arteriosclerosis, T., Vascular Biology Council on Cardiovascular, R., Intervention Council on Hypertension Council on, L., Cardiometabolic, H., 2023. The Neurovasculome: Key Roles in Brain Health and Cognitive Impairment: A Scientific Statement From the American Heart Association/American Stroke Association. Stroke. 54**,** e251-e271.
Jantti, H., Sitnikova, V., Ishchenko, Y., Shakirzyanova, A., Giudice, L., Ugidos, I. F., Gomez-Budia, M., Korvenlaita, N., Ohtonen, S., Belaya, I., Fazaludeen, F., Mikhailov, N., Gotkiewicz, M., Ketola, K., Lehtonen, S., Koistinaho, J., Kanninen, K. M., Hernandez, D., Pebay, A., Giugno, R., Korhonen, P., Giniatullin, R., Malm, T., 2022. Microglial amyloid beta clearance is driven by PIEZO1 channels. J Neuroinflammation. 19**,** 147.
Klement, W., Blaquiere, M., Zub, E., deBock, F., Boux, F., Barbier, E., Audinat, E., Lerner-Natoli, M., Marchi, N., 2019. A pericyte-glia scarring develops at the leaky capillaries in the hippocampus during seizure activity. Epilepsia. 60**,** 1399-1411.
Lee, W., Nims, R. J., Savadipour, A., Zhang, Q., Leddy, H. A., Liu, F., McNulty, A. L., Chen, Y., Guilak, F., Liedtke, W. B., 2021. Inflammatory signaling sensitizes Piezo1 mechanotransduction in articular chondrocytes as a pathogenic feed-forward mechanism in osteoarthritis. Proc Natl Acad Sci U S A. 118.
Lewis, S., 2023. Mechanics of amyloid clearance. Nat Rev Neurosci. 24**,** 1.
Li, J., Hou, B., Tumova, S., Muraki, K., Bruns, A., Ludlow, M. J., Sedo, A., Hyman, A. J., McKeown, L., Young, R. S., Yuldasheva, N. Y., Majeed, Y., Wilson, L. A., Rode, B., Bailey, M. A., Kim, H. R., Fu, Z., Carter, D. A., Bilton, J., Imrie, H., Ajuh, P., Dear, T. N., Cubbon, R. M., Kearney, M. T., Prasad, R. K., Evans, P. C., Ainscough, J. F., Beech, D. J., 2014. Piezo1 integration of vascular architecture with physiological force. Nature. 515**,** 279-282.
Liu, H., Hu, J., Zheng, Q., Feng, X., Zhan, F., Wang, X., Xu, G., Hua, F., 2022. Piezo1 Channels as Force Sensors in Mechanical Force-Related Chronic Inflammation. Front Immunol. 13**,** 816149.
Liu, T., Zhang, L., Joo, D., Sun, S. C., 2017. NF-kappaB signaling in inflammation. Signal Transduct Target Ther. 2**,** 17023-.
Marques, T. E., de Mendonca, L. R., Pereira, M. G., de Andrade, T. G., Garcia-Cairasco, N., Paco-Larson, M. L., Gitai, D. L., 2013. Validation of suitable

reference genes for expression studies in different pilocarpine-induced models of mesial temporal lobe epilepsy. PLoS One. 8**,** e71892.
Pernot, F., Heinrich, C., Barbier, L., Peinnequin, A., Carpentier, P., Dhote, F., Baille, V., Beaup, C., Depaulis, A., Dorandeu, F., 2011. Inflammatory changes during epileptogenesis and spontaneous seizures in a mouse model of mesiotemporal lobe epilepsy. Epilepsia. 52**,** 2315-25.
Riban, V., Bouilleret, V., Pham-Le, B. T., Fritschy, J. M., Marescaux, C., Depaulis, A., 2002. Evolution of hippocampal epileptic activity during the development of hippocampal sclerosis in a mouse model of temporal lobe epilepsy. Neuroscience. 112**,** 101-11.
Saotome, K., Murthy, S. E., Kefauver, J. M., Whitwam, T., Patapoutian, A., Ward, A. B., 2018. Structure of the mechanically activated ion channel Piezo1. Nature. 554**,** 481-486.
Schwarz, A. P., Kovalenko, A. A., Malygina, D. A., Postnikova, T. Y., Zubareva, O. E., Zaitsev, A. V., 2020. Reference Gene Validation in the Brain Regions of Young Rats after Pentylenetetrazole-Induced Seizures. Biomedicines. 8.
Shinge, S. A. U., Zhang, D., Din, A. U., Yu, F., Nie, Y., 2022. Emerging Piezo1 signaling in inflammation and atherosclerosis; a potential therapeutic target. Int J Biol Sci. 18**,** 923-941.
Streit, W. J., Khoshbouei, H., Bechmann, I., 2020. Dystrophic microglia in late-onset Alzheimer's disease. Glia. 68**,** 845-854.
Takata, K., Kozaki, T., Lee, C. Z. W., Thion, M. S., Otsuka, M., Lim, S., Utami, K. H., Fidan, K., Park, D. S., Malleret, B., Chakarov, S., See, P., Low, D., Low, G., Garcia-Miralles, M., Zeng, R., Zhang, J., Goh, C. C., Gul, A., Hubert, S., Lee, B., Chen, J., Low, I., Shadan, N. B., Lum, J., Wei, T. S., Mok, E., Kawanishi, S., Kitamura, Y., Larbi, A., Poidinger, M., Renia, L., Ng, L. G., Wolf, Y., Jung, S., Onder, T., Newell, E., Huber, T., Ashihara, E., Garel, S., Pouladi, M. A., Ginhoux, F., 2017. Induced-Pluripotent-Stem-Cell-Derived Primitive Macrophages Provide a Platform for Modeling Tissue-Resident Macrophage Differentiation and Function. Immunity. 47**,** 183-198 e6.
Turovsky, E. A., Braga, A., Yu, Y., Esteras, N., Korsak, A., Theparambil, S. M., Hadjihambi, A., Hosford, P. S., Teschemacher, A. G., Marina, N., Lythgoe, M. F., Haydon, P. G., Gourine, A. V., 2020. Mechanosensory Signaling in Astrocytes. J Neurosci. 40**,** 9364-9371.
Tyler, W. J., 2012. The mechanobiology of brain function. Nat Rev Neurosci. 13**,** 867-78.
van Vliet, E. A., Marchi, N., 2022. Neurovascular unit dysfunction as a mechanism of seizures and epilepsy during aging. Epilepsia. 63**,** 1297-1313.
Velasco-Estevez, M., Koch, N., Klejbor, I., Caratis, F., Rutkowska, A., 2022. Mechanoreceptor Piezo1 Is Downregulated in Multiple Sclerosis Brain and Is Involved in the Maturation and Migration of Oligodendrocytes in vitro. Front Cell Neurosci. 16**,** 914985.
Velasco-Estevez, M., Rolle, S. O., Mampay, M., Dev, K. K., Sheridan, G. K., 2020. Piezo1 regulates calcium oscillations and cytokine release from astrocytes. Glia. 68**,** 145-160.
Vezzani, A., Balosso, S., Ravizza, T., 2019. Neuroinflammatory pathways as treatment targets and biomarkers in epilepsy. Nat Rev Neurol. 15**,** 459-472.
Vezzani, A., Ravizza, T., Bedner, P., Aronica, E., Steinhauser, C., Boison, D., 2022. Astrocytes in the initiation and progression of epilepsy. Nat Rev Neurol. 18**,** 707-722.

Yang, K., He, X., Wu, Z., Yin, Y., Pan, H., Zhao, X., Sun, T., 2022. The emerging roles of piezo1 channels in animal models of multiple sclerosis. Front Immunol. 13**,** 976522.
Zhang, Y., Wang, G., Xie, M., Lian, L., Xiong, Y., Xu, F., Li, G., Tang, Z., Wang, F., Zhu, S., 2022. Piezo1 Mediates Inflammation in Balloon-inflated Rat Brain and its Bidirectional Mechanosensitivity. Curr Mol Med.